• Basic Research •

Integrating multiple key molecules in uveal melanoma to uncover metastatic and immune microenvironment-related gene signatures

Yi-Ming Guo[1], *Zhan-Pei Bai*[2], *Jia-Qi Wang*[1], *Juan Huang*[1], *Jun-Han Wei*[1], *Yi-Jin Han*[1], *Yang Liu*[3], *Lu Ye*[1]

[1]Shaanxi Eye Hospital, Xi'an People's Hospital (Xi'an Fourth Hospital), Affiliated People's Hospital of Northwest University, Xi'an 710004, Shaanxi Province, China
[2]The Second Affiliated Hospital of Wenzhou Medical University, Wenzhou Medical University, Wenzhou 325000, Zhejiang Province, China
[3]People's Hospital of Ningxia Hui Autonomous Region, Ningxia Medical University, Ningxia Clinical Research Institute, Yinchuan 750000, Ningxia Hui Autonomous Region, China

Correspondence to: Lu Ye. Shaanxi Eye Hospital, Xi'an People's Hospital (Xi'an Fourth Hospital), Affiliated People's Hospital of Northwest University, Xi'an 710004, Shaanxi Province, China. YL0618@med.nwu.edu.cn; Yang Liu. People's Hospital of Ningxia Hui Autonomous Region, Ningxia Medical University, Ningxia Clinical Research Institute, Yinchuan 750000, Ningxia Hui Autonomous Region, China. herbliuyang@163.com

Received: 2025-07-04 Accepted: 2025-09-05

Abstract

● **AIM:** To identify metastasis-associated prognostic genes and construct a robust molecular signature for survival prediction in uveal melanoma (UVM) patients.

● **METHODS:** Transcriptomic data and clinical information from 80 UVM patients in the Cancer Genome Atlas (TCGA)-UVM cohort and an external Gene Expression Omnibus (GEO) microarray dataset (GSE73652; 8 non-metastatic *vs* 5 metastatic cases) were analyzed to identify differentially expressed genes (DEGs). Functional enrichment, protein-protein interaction (PPI) network construction, and survival analyses identified seven metastasis- and prognosis-related genes. Their expression was further examined using public single-cell RNA-seq data (GSE139829; 11 tumors). Experimental validation was performed in UVM cell lines (92.1, OMM1, MEL270) and adult retinal pigment epithelial (ARPE-19) cells using quantitative real-time polymerase chain reaction (qRT-PCR) and Western blotting to confirm transcriptomic trends. A LASSO Cox model was applied to construct a metastasis-related risk Score signature. Tumor immune microenvironment characteristics were evaluated *via* single-sample gene set enrichment analysis (ssGSEA) and ESTIMATE. Somatic mutation and copy number variation (CNV) profiles were also examined.

● **RESULTS:** Seven key genes (*UBE2T*, *KIF20A*, *DLGAP5*, *KLC3*, *TPX2*, *UBE2C*, *AURKA*) were significantly associated with overall survival and used to construct a metastasis-related riskScore signature, which effectively stratified patients into high- and low-risk groups and served as an independent prognostic factor. qRT-PCR and Western blot results confirmed that the expression levels of selected key genes in UVM cell lines showed significant differences compared to ARPE-19 cells, which were largely consistent with the transcriptomic findings. The high-risk group exhibited reduced immune infiltration and stromal activity. Single-cell analysis revealed these genes were predominantly expressed in a tumor cell cluster characterized by BAP1 loss and high metastatic potential. Mutation and CNV analyses further supported the relevance of these genes to UVM progression.

● **CONCLUSION:** This study establishes and validates a seven-gene signature associated with metastasis and prognosis in UVM. The findings provide a framework for understanding molecular determinants of tumor progression and immune microenvironment alterations, and may offer guidance for future mechanistic studies and therapeutic exploration.

● **KEYWORDS:** uveal melanoma; RNA-seq; immune analysis; survival analysis; single-cell RNA

DOI:10.18240/ijo.2026.01.02

Citation: Guo YM, Bai ZP, Wang JQ, Huang J, Wei JH, Han YJ, Liu Y, Ye L. Integrating multiple key molecules in uveal melanoma to uncover metastatic and immune microenvironment-related gene signatures. *Int J Ophthalmol* 2026;19(1):11-24

INTRODUCTION

Uveal melanoma (UVM), including choroidal and iris melanoma, represents a formidable primary intraocular malignancy originating from melanocytes[1]. It accounts for 3%-5% of all melanomas cases and about 95% of ocular melanomas, which is the most common primary intraocular malignancy in adults[2]. UVM is usually asymptomatic and imperceptible, and only a few patients develop visual symptoms as the disease progresses, such as flickers, floaters, or visual field defects, and even some are found in routine eye exams[3].

At present, the clinical treatment of UVM includes not only traditional resection and radiotherapy, but also the increasingly updated targeted therapy, immunotherapy and other therapeutics, as well as targeted disease biology and risk stratification, adjuvant therapy options and metastatic disease treatment strategies, bringing UVM treatment to new heights and requirements[4-5]. However, the high metastasis of UVM from eye to other organs poses new challenges to its treatment and patient prognosis[3]. For example, nearly 50% of UVM patients can develop tumor metastasis through hematogenous dissemination to the liver. In the first five years after primary UVM diagnosis, 15% to 20% of patients succumb to systemic metastases, while 45% meet the same fate within 15y of initial diagnosis[6]. Regrettably, prevailing interventions demonstrate limited efficacy in thwarting distant metastatic occurrences[7-8]. Against this backdrop, a comprehensive exploration of the mechanisms underpinning UVM metastasis emerges as a compelling imperative[9]. Such endeavors not only deepen our comprehension of UVM's pathogenesis and progression but also wield profound implications for refining clinical interventions and enhancing prognostic precision for individuals afflicted by UVM.

Tumor progression is profoundly influenced by the surrounding microenvironment, wherein complex bidirectional interactions facilitate immune evasion, tumor proliferation, and metastatic dissemination[10]. The tumor milieu is characterized by infiltration of diverse immune cell populations, with compelling evidence supporting their critical involvement in tumor initiation and advancement[11-12]. Both immune and stromal components have been demonstrated to significantly modulate patient survival outcomes across various cancers[13]. In UVM, a subset of tumors exhibits pronounced immune infiltration marked by elevated interferon-gamma signaling, which correlates with adverse prognosis[14-15]. Furthermore, neutrophils have emerged as important prognostic indicators, showing strong associations with key prognostic genes and $CD8^+$ T cell infiltration[16]. Notably, specific immune cell subsets are enriched within metastatic UVM tissues, underscoring the pivotal role of immune dynamics in the metastatic cascade[17]. These observations suggest that disruption of immune homeostasis may underlie metastatic progression in UVM. Collectively, alterations in the immune microenvironment during choroidal melanoma metastasis carry significant implications for patient prognosis and therapeutic strategies.

In this study, we developed gene signatures specifically associated with UVM metastasis and the tumor immune microenvironment. By identifying and integrating key molecular regulators, we aimed to establish a comprehensive framework that not only correlates with clinical outcomes in UVM patients but also delineates the unique immunological landscape of the disease. Building upon these signatures, we constructed predictive models for clinical validation and further explored the functional relevance of these molecules through analyses at the single-cell transcriptomic and copy number variation levels. Overall, our findings highlight the potential utility of these gene signatures to advance understanding and prognostic evaluation of UVM metastasis.

MATERIALS AND METHODS

Ethical Approval All bioinformatic analyses in this study were based on publicly available datasets, including The Cancer Genome Atlas (TCGA)-UVM (https://portal.gdc.cancer.gov/), GSE13911, and GSE73652 from the Gene Expression Omnibus (GEO) database. No patient recruitment or animal experiments were conducted. For experimental validation, the human UVM cell line 92.1 and the normal retinal pigment epithelial cell line adult retinal pigment epithelial (ARPE-19) were commercially obtained from AcceGen Biotechnology (Fairfield, NJ, USA). All experimental procedures were reviewed and approved by the Ethics Committee of Xi'an People's Hospital (Xi'an Fourth Hospital), under approval number KJLLZ-K-2025021.

Data Mining From the Cancer Genome Atlas Database and Gene Expression Omnibus Database The gene expression profiles and the corresponding clinical data of 80 UVM patients were downloaded from the University of California Santa Cruz (UCSC) Xena browser (https://xenabrowser.net/) with cohort name: TCGA-UVM. Single-cell transcriptome files of GSE139829 were downloaded from the GEO database (http://www.ncbi.nlm.nih.gov/geo/). Mutation annotation files were downloaded from TCGA database (https://www.cancer.gov/ccg/research/genome-sequencing/tcga). Besides, a microarray dataset, GSE73652 (platform GPL10558, Illumina HumanHT-12 V4.0 expression beadchip Illumina, Inc., San Diego, CA, United States), was also downloaded from GEO database.

Differentially Expressed Gene Analysis To identify the key molecules associated with tumor metastasis, we used the limma package to screen the DEGs between Class 1 (low metastatic risk) and Class 2 (high metastatic risk)[18]. The cut-off criteria were P value <0.05 and $|\log_2 FC>1|$ for DEGs.

Gene Ontology and Kyoto Encyclopedia of Genes and Genomes Pathway Functional Enrichment Analysis of DEGs To annotate the potential function and biological processes (BP) of these DEGs, we performed GO and KEGG enrichment analysis by using the clusterProfiler R package. The GO enrichment analysis was conducted based on three aspects including BP, molecular functions (MF) and cellular components (CC), and the results were visualized using the "cnetplots" R package. The differentially expressed genes were categorized into up-regulated and down-regulated DEGs groups. Significantly relevant signal pathways were identified using R software. The categorized groups were analyzed and presented using bar graphs.

Protein-Protein Interaction Network and Module Analysis The STRING (http://string-db.org/) was used to comprehensively analyze the interaction between the DEGs. Cytoscape (http://www.cytoscape.org/) was applied for visualization of protein-protein interaction (PPI) network of the DEGs. Using Cytoscape's plugin Cytohubba, we selected the top 50 DEGs with high connectivity in the gene expression network as the hub genes according to the degree algorithm. The clustered sub-networks and modules of the hub genes from the PPI network were searched by the Cytoscape MCODE plug-in[19].

Survival Analysis Survival significance of the top 50 hub genes was evaluated using Kaplan-Meier analysis and univariate Cox proportional hazards regression. Log-rank tests were used to calculate *P*-values for the survival curves, and genes with $P<0.05$ and hazard ratios not equal to 1 were considered prognostically relevant and selected for downstream analyses.

Cell Lines and Culture Conditions The human UVM cell line 92.1 and ARPE-19 were procured from AcceGen Biotechnology (Fairfield, NJ, USA). 92.1 cells were cultured in a complete medium specific to the cell line (Zhongqiao Xinzhou Biotechnology, Shanghai, China; Cat# ZM1129). ARPE-19 cells were maintained in Dulbecco's modified Eagle medium (DMEM) supplemented with 10% fetal bovine serum (FBS), 1% penicillin–streptomycin (100 U/mL and 100 μg/mL), and 2 mmol/L L-glutamine. Cultures were maintained at 37°C in a humidified incubator with 5% CO_2 and were routinely tested for mycoplasma contamination.

RNA Extraction and Quantitative Real-Time PCR Total RNA was isolated using TRIzol reagent (Invitrogen, USA) following the manufacturer's instructions. The purity and concentration of extracted RNA were determined with a NanoDrop 2000 spectrophotometer (Thermo Fisher Scientific, USA). Complementary DNA (cDNA) was synthesized from 1 μg of total RNA using the PrimeScript™ RT reagent kit (Takara Bio, Japan). Quantitative real-time polymerase chain reaction (PCR) was conducted using SYBR Green qPCR Master Mix (Vazyme, China) on an ABI 7500 Fast Real-Time PCR System (Applied Biosystems, USA). GAPDH was employed as the endogenous reference gene. Relative gene expression levels were calculated *via* the $2^{-\Delta\Delta Ct}$ method. Each sample was analyzed in triplicate to ensure reproducibility.

Protein Extraction and Western Blotting Cells were lysed using RIPA lysis buffer (Beyotime, China) supplemented with protease and phosphatase inhibitor cocktails (MedChemExpress, China). Protein concentration was quantified using the BCA Protein Assay Kit (Beyotime, China). Equal amounts of protein (30-50 μg) were separated on 10%-12% SDS-PAGE gels and transferred onto polyvinylidene difluoride (PVDF) membranes (Millipore, USA). Membranes were blocked in 5% non-fat milk in tris-buffered saline with Tween (TBST) for 1h at room temperature and then incubated overnight at 4°C with primary antibodies against UBE2T, KIF20A, DLGAP5, KLC3, TPX2, UBE2C, AURKA (Proteintech, China or Abcam, UK), and GAPDH (Cell Signaling Technology, USA) as a loading control. After washing, membranes were incubated with horseradish peroxidase (HRP)-conjugated secondary antibodies (Jackson ImmunoResearch, USA) for 1h at room temperature. Protein bands were visualized using enhanced chemiluminescence (ECL) reagents (Tanon™, China) and imaged with a ChemiDoc XRS+ system (Bio-Rad, USA). Densitometric analysis was conducted using Image J software (NIH, USA).

Inference of Tumor Microenvironment Infiltration Cells To characterize the immune composition within the tumor microenvironment (TME), we employed the single-sample gene set enrichment analysis (ssGSEA) method, incorporating immune-related gene signatures curated from the CIBERSORT algorithm[20]. To minimize the potential confounding effects of tumor purity, immune cell infiltration scores were corrected using the ESTIMATE algorithm[21]. The resulting normalized enrichment scores served as proxies for the relative abundance of 24 immune cell populations in each sample.

Generation of Prognostic Signatures Based on Key Molecules A metastasis-related prognostic model (riskScore) was developed based on the expression of seven signature genes. LASSO Cox regression was used to reduce dimensionality and select optimal predictors[22]. The risk score was computed as follows:

$$Risksocre=\Sigma N_i=1(Coef_i\times Exp_i)$$

where $Coef_i$ was the coefficient obtained from LASSO Cox regression and $Expr_i$ was the expression of signature genes.

Single-cell RNA-sequencing Analysis Single-cell data (GSE139829) were integrated using Seurat. Cells with <400 or >10 000 features, <100 or >8000 counts, or >10% mitochondrial content were excluded. Following normalization with the LogNormalize method and batch correction using Harmony, we retained 52 228 cells from eight primary

and three metastatic UVM tumors. PCA was applied for dimensionality reduction, followed by UMAP and t-distributed stochastic neighbor embedding (t-SNE) visualization. Clustering was performed with the FindClusters function (resolution=0.1), and clusters were annotated based on canonical markers.

Gene Set Enrichment Analysis Analysis Gene Set Enrichment Analysis (GSEA) was used to identify pathway enrichment differences between primary and metastatic UVM samples. KEGG gene sets were obtained from the MSigDB database, and pathways with nominal *P*-values<0.05 were deemed significant[23].

Gene Mutation Analysis To investigate the genomic alterations associated with the prognostic gene signature, we performed a comprehensive analysis of somatic mutation data derived from the TCGA-UVM cohort using the maftools package in R[24]. Based on the riskScore computed *via* LASSO regression, patients were categorized into high- and low-risk subgroups. Subsequently, genome-wide copy number variations (CNVs) were analyzed using the GISTIC2.0 algorithm, enabling identification of chromosomal regions exhibiting statistically significant amplifications or deletions[25-26].

Statistical Analysis All computational and statistical analyses were performed in R (version 4.1.3). Correlation relationships were assessed using both Spearman's rank correlation and distance correlation methods. Univariate Cox proportional hazards regression models were employed to calculate hazard ratios (HRs) and corresponding 95% confidence intervals (CIs), while multivariate Cox regression analyses were conducted to determine the independent prognostic significance of the risk score signature. Experimental data derived from quantitative real-time polymerase chain reaction (qRT-PCR) and Western blot assays are presented as mean±standard deviation (SD) based on a minimum of three independent biological replicates. Comparisons between groups were conducted using either Student's *t*-test or one-way analysis of variance (ANOVA), depending on the experimental design. All statistical tests were two-tailed, and a *P*-value less than 0.05 was considered indicative of statistical significance.

RESULTS

Identification of Metastasis-Related Prognostic Regulators The comprehensive analysis process is summarized in Figure 1A. The microarray data underwent normalization before analysis. Following the processing of the array expression profile, PCA was employed, revealing discernible distinctions among the 11 samples of two groups. Notably, a total of 651 genes exhibited significantly different expressions in tumor samples compared to normal samples. These differences were based on the comparison of 8 non-metastatic samples and 5 metastatic samples, with a threshold of *P* value <0.05 and $|\log_2 FC| \geq 1$. Among them, 358 genes were down-regulated, while 293 genes were up-regulated (Figure 1B). GO analysis highlighted that the DEGs were predominantly enriched in functions like organelle fission, nuclear division, microtubule and microtubule associated complex, indicating an association between UVM with high metastatic risk and cell division and proliferation (Figure 1C). Furthermore, KEGG analysis revealed that up-regulated genes were significantly enriched in pathways, including cell cycle and endocrine resistance, while down-regulated genes participated in diverse other pathways (Figure 1D).

Selection of Key Genes for Prognostic Evaluation To identify key molecular regulators associated with UVM metastasis, we first constructed a PPI network based on the DEGs, which revealed a high degree of connectivity among metastasis-related candidates. Using the cytoHubba plugin in Cytoscape, the top 50 hub genes were identified and visualized (Figure 1E). These genes were then subjected to univariate Cox regression and Kaplan–Meier survival analyses, and seven genes—*UBE2T*, *KIF20A*, *DLGAP5*, *KLC3*, *TPX2*, *UBE2C*, and *AURKA*—were significantly associated with overall survival (*P*<0.05 and HR≠1). The expression profiles of these seven genes differed markedly between metastatic and non-metastatic UVM samples (Figure 1F).

To further validate the differential expression of these candidate genes at the transcript and protein levels, we performed qRT-PCR and Western blot analyses in the human UVM cell line 92.1 and the normal retinal pigment epithelial cell line ARPE-19. The results demonstrated that the expression levels of several key genes were significantly altered in 92.1 cells compared to ARPE-19, with trends consistent with transcriptomic data from the TCGA-UVM cohort (Figure 2A-2B). These genes were further highlighted in the volcano plot of all DEGs (Figure 2D).

PCA distinctly segregated UVM patients into high- and low-risk clusters according to the expression patterns of the seven selected genes (Figure 2E). Furthermore, Spearman correlation analysis revealed robust positive associations among these genes, implying their potential co-regulatory roles in the metastatic progression of UVM (Figure 2F).

Exploration of Tumor Microenvironment Immune Cell Infiltration The landscape of 24 TME cell infiltrations was evaluated in normal and malignant samples, shedding light on the functions of the crucial molecules in TME immune cell infiltration. Of the 24 TME cell types, only six (type 1 T helper cells, type 2 T helper cells, activated CD4 T cells, gamma delta T cells, effector memory CD8 T cells, and plasmacytoid dendritic cells) displayed statistically significant differences in infiltration between normal and tumor samples,

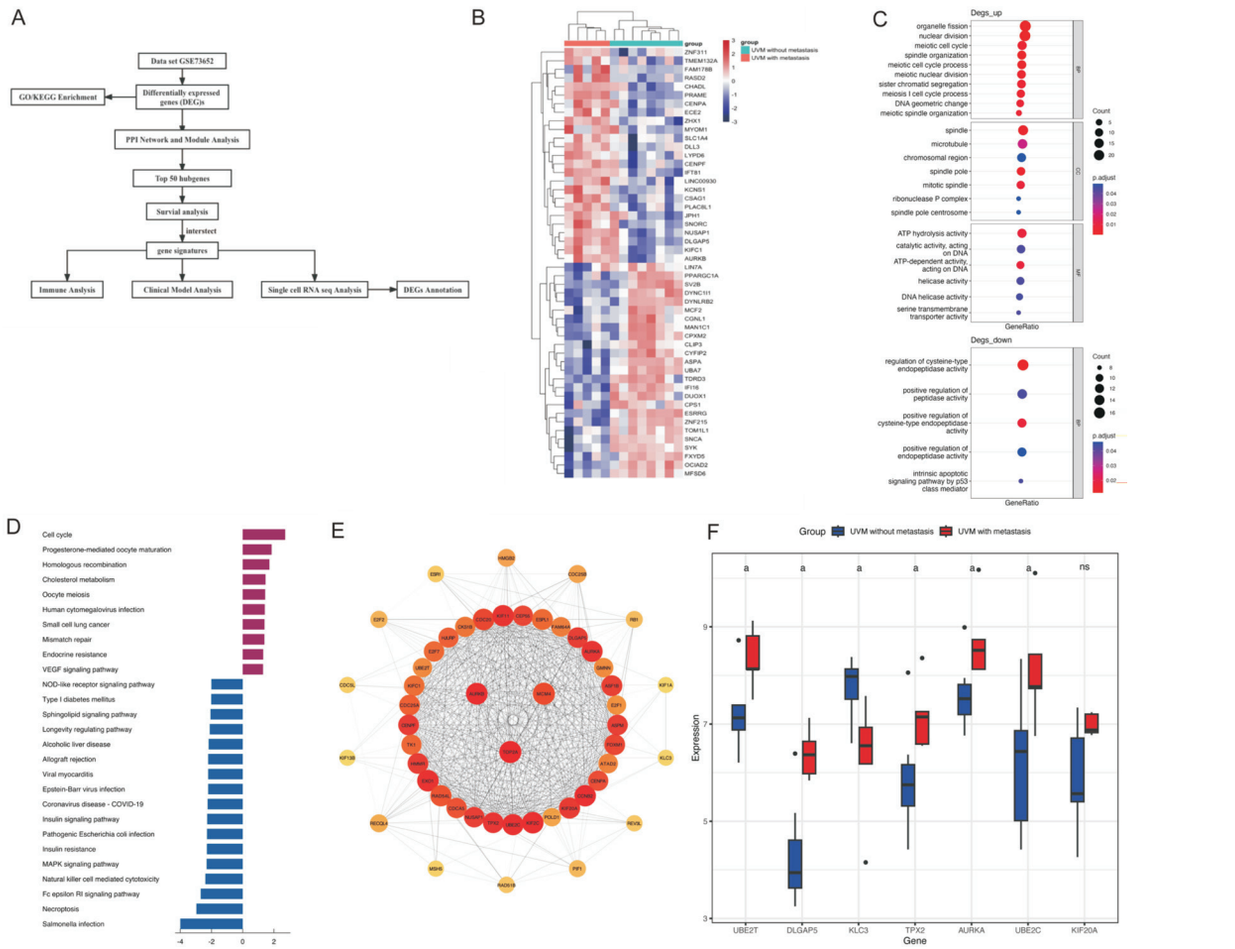

Figure 1 Differentially expressed genes analysis and annotation of UVM with Class 1 (low metastatic risk) and Class 2 (high metastatic risk) A: Schematic workflow illustrating the overall analytical strategy of the study. B: Heatmap visualizing the top 25 upregulated and downregulated DEGs between Class 1 and Class 2 tumor groups, based on $|\log_2(\text{fold change})|>1$ and $P<0.05$. C, D: Bar plots representing significantly enriched biological processes and pathways identified through GO and KEGG analyses of DEGs, colored by adjusted *P*-values. E: Visualization of the top 50 hub genes with the highest connectivity scores, identified using the CytoHubba plugin in Cytoscape. F: Relative expression levels of the seven key genes in Class 1 and Class 2 UVM groups. Statistical significance is denoted as follows: ns (not significant), $^{a}P<0.05$. GO: Gene Ontology; KEGG: Kyoto Encyclopedia of Genes and Genomes; DEGs: Differentially expressed genes; UVM: Uveal melanoma.

all of which exhibited low levels of infiltration (Figure 3A). And the result corresponded to the phenomenon that UVM is largely unresponsive to checkpoint immunotherapy. Principal Component Analysis (PCA) further indicated distinct TME cell population shifts, highlighting potential implications for UVM metastasis, immune evasion, and immunotherapy resistance (Figure 3B). The ESTIMATE method was used to gauge immune and stromal activity, revealing significantly lower activity levels in tumors compared to healthy uveal tissues (Figure 3C). Correlation analysis revealed an inverse association between important genes and TME-infiltrating cells. However, activated memory CD4 T cell infiltration displayed a strong positive correlation with the seven key molecules (Figure 3D).

Construction of Prognostic Gene Signatures The prognostic impact of the gene signature was evident through Kaplan-Meier curve. To enhance the clinical relevance, a riskScore signature was developed using the LASSO Cox regression model, incorporating the roles of the seven key molecules. The expression of the three most representative important molecules, *KIF20A*, *DLGAP5*, and *KLC3*, contributed to the riskscore calculation (Figure 4A-4B). Patients were categorized into high- and low-risk groups using the MaxStat R package's cutoff value of 0.30 (Figure 4C). Notably, patients in the low-risk group exhibited improved survival outcomes (Figure 4D). The expression of seven important molecules in cancers with high risk was statistically different from that of tumors with low risk (Figure 4E). Patient mortality demonstrated a clear increase with elevated risk levels (Figure 4F). Age, gender, clinical stage, and T stage were all included in the multivariate Cox regression model analysis and the result showed that riskScore signature could serve as a reliable and independent predictive biomarker for assessing UVM patient outcomes (Figure 4G). A nomogram was constructed

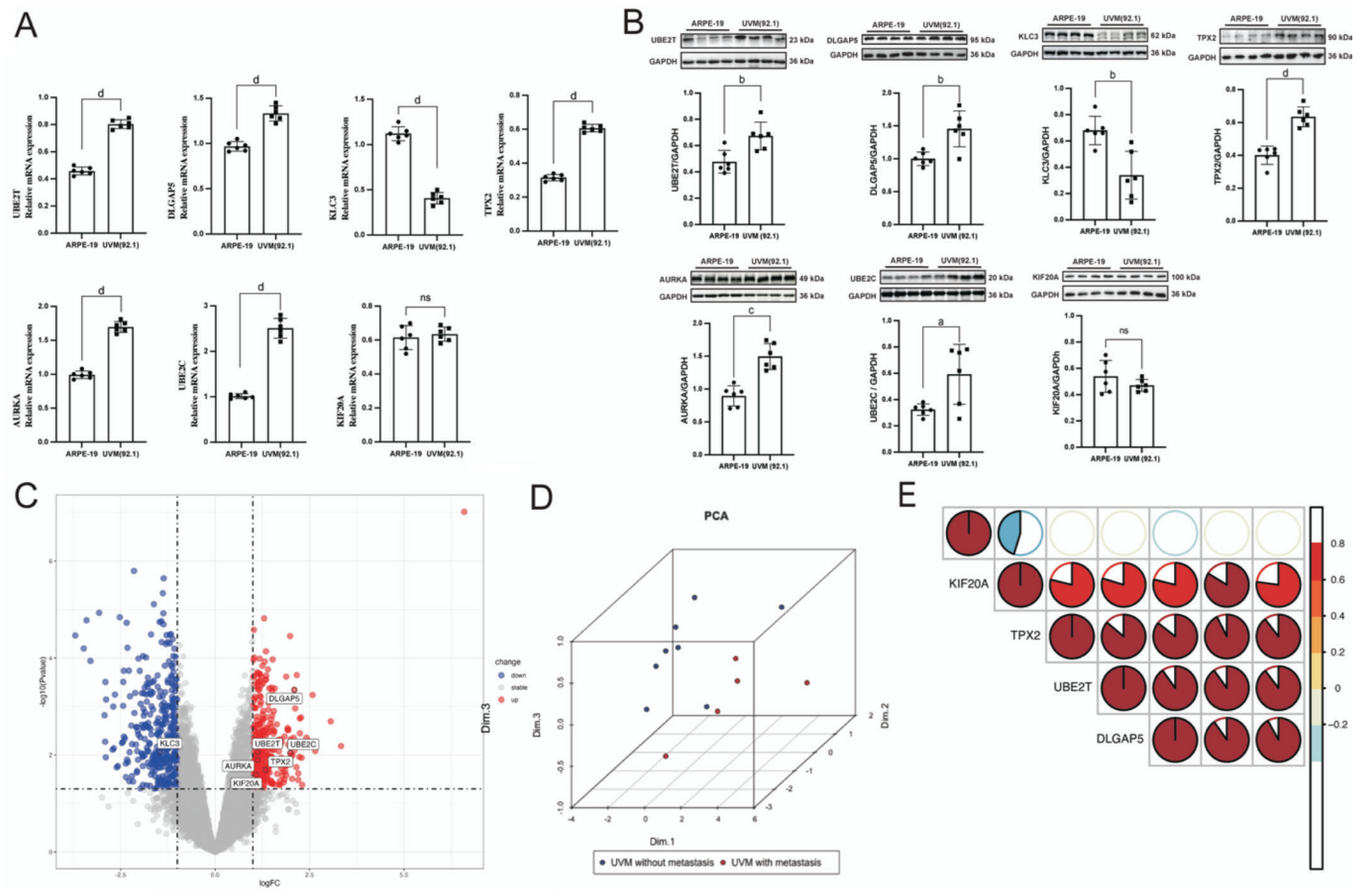

Figure 2 Identification of prognostic metastasis-related signature in UVM cohort A: qRT-PCR validation of mRNA expression levels of the seven key genes in 92.1 cells compared to ARPE-19 cells. B: Western blot analysis and densitometric quantification of protein expression levels of the seven key genes in 92.1 and ARPE-19 cells. Data are presented as mean±SD from three independent experiments. Statistical significance was assessed using unpaired Student's *t*-test: ns (not significant), [a]*P*<0.05, [b]*P*<0.01, [c]*P*<0.001, and [d]*P*<0.0001. C: Volcano plot of DEGs in the GSE73652 dataset, with the seven selected key genes highlighted. D: PCA based on the expression of the seven key genes revealed distinct clustering of high- and low-risk samples. E: Spearman correlation analysis among the seven key genes. Positive correlations are indicated in red, and negative correlations in blue. qRT-PCR: Quantitative real-time polymerase chain reaction; DEGs: Differentially expressed genes; UVM: Uveal melanoma; PCA: Principal component analysis; SD: Standard deviation; ARPE-19: Adult retinal pigment epithelium.

by integrating riskScore and independent clinical prognostic indicators, providing a clinically relevant tool for estimating patient mortality likelihood. Calibration plots confirmed the performance of the derived nomogram (Figure 4H-4I).

Exploration of Gene Signatures in Single-Cell Expression

scRNA-seq has become an indispensable approach to dissect the cellular heterogeneity and molecular characteristics within tumors. To gain an in-depth understanding of the malignant landscape of UVM, we evaluated the expression patterns of candidate gene signatures at the single-cell level. Utilizing the publicly available GSE139829 dataset from GEO, which comprises samples from eight metastatic and eight primary UVM tumors, we explored the cellular complexity within this cancer type. After stringent quality filtering, normalization, and integration using the Seurat and Harmony algorithms, a total of 434 569 cells from 11 patients were included for downstream analysis. Dimensionality reduction *via* UMAP uncovered a heterogeneous array of tumor cell populations (Figure 5A). Subsequent identification of cluster-specific marker genes yielded 5229 genes distributed across ten distinct clusters (Figure 5B), reflecting the notable intratumoral diversity of UVM. Notably, the six key hub genes were primarily enriched in cluster 5 (Figure 5C). Cell-type annotation, performed by combining the FindAllMarkers function and established marker gene knowledge, enabled accurate characterization of clusters (Figure 5D). For instance, cluster 0 was defined by canonical B cell markers CD19, CD79A, and MS4A1, whereas cluster 4 corresponded to plasma cells, marked by IGHG1, MZB1, and SDC1 (Figure 5E). Of particular interest, we identified two tumor cell subsets distinguished by marker expression: Tumor cells-1, characterized by MLANA, MITF, and DCT, and Tumor cells-2, defined by STMN1 and TYMS expression. Importantly, the hub genes under investigation exhibited predominant expression in Tumor cells-2, which has been previously implicated as the BAP1-mutant, high metastatic risk tumor cell population (Figure 5F).

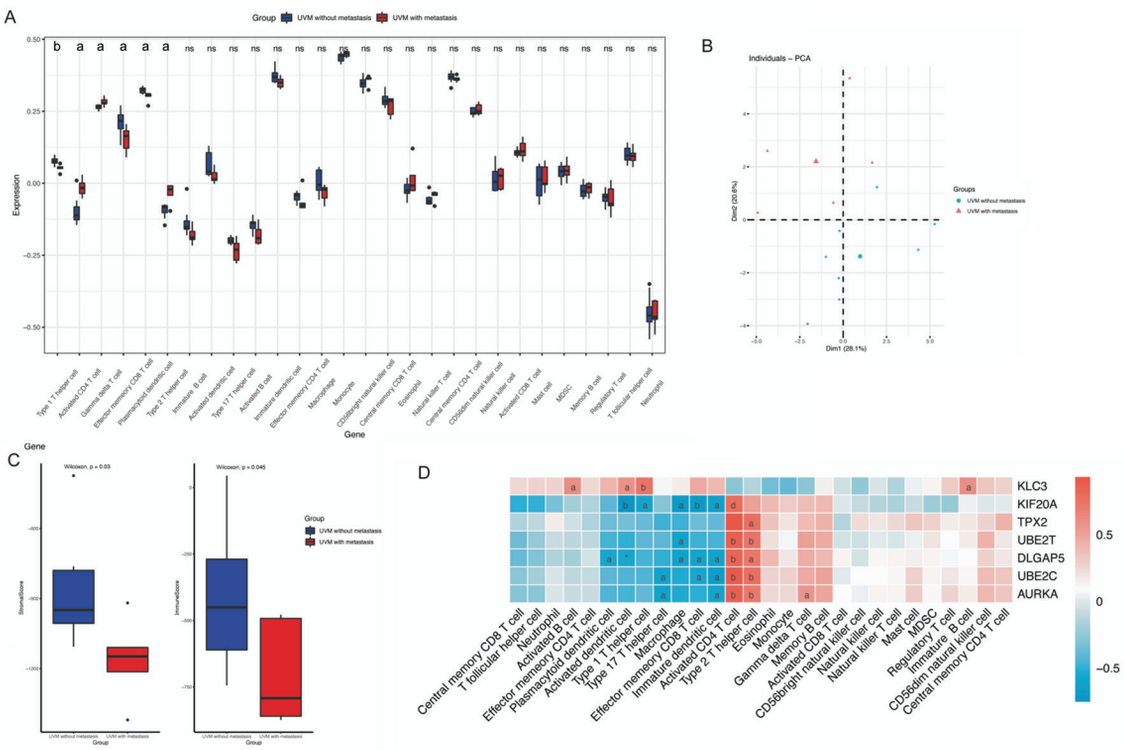

Figure 3 Evaluation of immune micro-environment characterization A: Comparative analysis of 24 TME-associated immune cell types between Class 1 and Class 2 tumor groups. Statistically significant differences are indicated ns (not significant), [a]*P*<0.05, [b]*P*<0.01. B: PCA based on the infiltration levels of the 24 immune cell populations revealed distinct clustering patterns between the two groups, indicating substantial immune landscape divergence. C: Evaluation of global immune and stromal cell infiltration using the ESTIMATE algorithm. Immune score comparison demonstrating overall immune suppression in tumor samples. D: Stromal score comparison indicating reduced stromal content in UVM tissues. D: Correlation matrix illustrating the relationship between each key prognostic gene and the abundance of specific TME-infiltrating immune cell subsets. TME: Tumor microenvironment; PCA: Principal component analysis; UVM: Uveal melanoma.

Gene Differential Analysis and Annotation of Tumor Clusters Given the preferential localization of these pivotal genes within Tumor cells-2, we isolated this cluster for more focused analyses. Further dimensionality reduction and clustering failed to reveal additional subpopulations with concentrated expression of these genes. Therefore, we proceeded to compare gene expression profiles between primary and metastatic UVM cells within Tumor cells-2. This comparative analysis identified 63 genes displaying statistically significant differential expression, encompassing both upregulated and downregulated genes, visualized through a heatmap representation (Figure 6A). GO enrichment analysis revealed that these differentially expressed genes are predominantly involved in immune-related processes, including regulation of B cell activation, intracellular protein localization, humoral immune responses, and complement activation pathways. These findings imply that the distinct gene expression changes within this tumor cell cluster may modulate the tumor immune microenvironment and contribute to the metastatic progression of UVM (Figure 6B).

KEGG pathway analysis indicated that the differentially expressed genes are implicated in multiple disease-related pathways. Notably, pathways associated with oxidative phosphorylation and cell adhesion molecules emerged as potentially critical in the metastatic behavior of UVM. These findings suggest that alterations in these BPs may contribute to the metastatic capacity of UVM tumor cells (Figure 6C).

Then GSEA analysis was used to further annotate the gene expression of the cluster, and the results showed that the related terms were classified into cell metastasis, immunity, metabolism, and chemical carcinogenicity, all of which could promote UVM deterioration (Figure 6D). For example, reduced cell adhesion promotes tumor cell metastasis, and genes in the metastasis group are down-regulated in this pathway; changes in the expression of genes involved in glucose metabolism could meet the needs of high metabolism of tumor cells, and these genes are up-regulated in the group of high-risk metastasis. In summary, the GSEA results give us a more specific understanding of the expression trends of all genes in each pathway, and these trends can help us to further study the mechanism of their development and metastasis in the future.

Understanding the Molecular Mechanism of Gene Signatures In this comprehensive study, we diligently

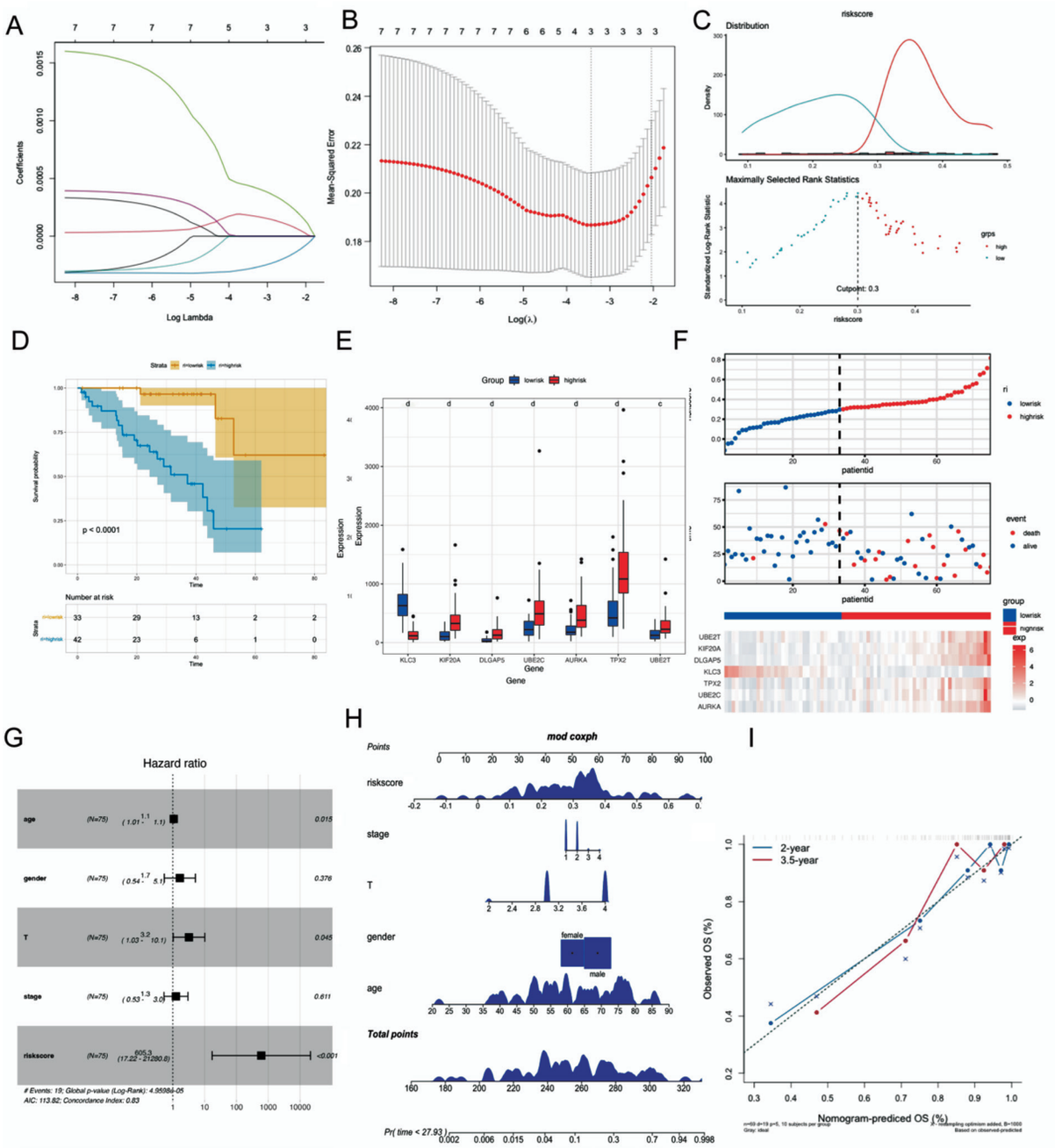

Figure 4 Validation of prognostic significance of selected gene signatures A: Coefficient profiles of the seven selected genes obtained *via* LASSO regression. B: Tenfold cross-validation was used to determine the optimal penalty parameter (λ) in the LASSO model, with the partial likelihood deviance plotted against log(λ). Vertical dashed lines indicate λ values selected by minimum criteria and the 1-standard error rule. C: The optimal threshold for stratifying patients into high- and low-risk groups was determined using the MaxStat algorithm (cut-off=0.30). D: Kaplan-Meier curves demonstrate significantly better overall survival in the low-risk group compared to the high-risk group (Log-rank test, P<0.05). E: Expression profiles of the seven genes across risk groups; statistical significance is denoted as ^{c}P<0.001, ^{d}P<0.0001). F: Risk score distribution among TCGA patients and hierarchical clustering of the seven key genes, along with the corresponding mortality trends across risk groups. G: Forest plot of multivariate Cox regression analysis indicates that the riskscore is an independent prognostic factor. H: Nomogram integrating riskscore and clinical parameters for individualized survival prediction in UVM patients. I: Calibration curves demonstrating concordance between predicted and observed survival at 2 and 3.5y. LASSO: Least absolute shrinkage and selection operator; TCGA: The Cancer Genome Atlas; UVM: Uveal melanoma; Riskscore: Metastasis-related risk score.

acquired the available somatic mutation profiles. Our focus was directed at analyzing the mutation landscapes within the high- and low-risk clusters derived from the TCGA-UVM dataset. The tool "oncoplot" facilitated this analysis, revealing the top 20 genes with notably high mutation frequencies in both groups(Figure 7A). Evidently, despite disparities in gene mutation frequencies, genes *GNAQ* and *GNA11* exhibited frequencies surpassing 30%. To further elucidate the

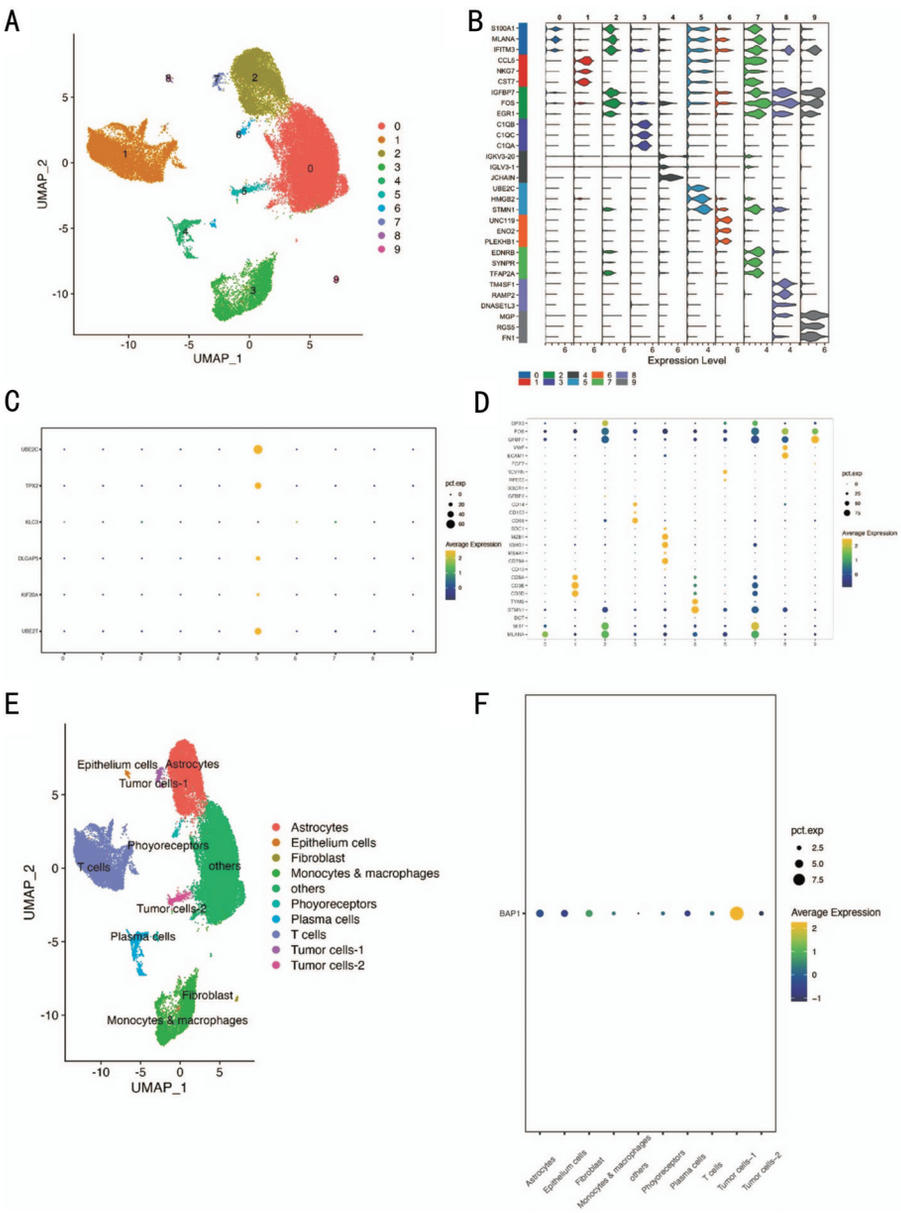

Figure 5 Evaluation of gene signatures at single-cell level A: Cell populations from UVM samples were projected using UMAP based on the top 20 principal components, resulting in ten transcriptionally distinct clusters. B: Heatmap summarizing cluster-defining marker genes, delineating the molecular characteristics of each cell group. C: Dot plot illustrating the distribution and expression levels of the selected metastasis-associated gene signature across all clusters. D: Cluster identities were inferred by evaluating the expression of established lineage-specific markers, as shown in the dot plot. E: UMAP visualization of annotated clusters derived from single-cell transcriptomes of 11 UVM patients, categorized according to classical marker gene profiles. F: Cluster-wise expression pattern of BAP1, emphasizing its selective enrichment within tumor subsets associated with metastatic potential. UMAP: Uniform Manifold Approximation and Projection; UVM: Uveal melanoma; BAP1: BRCA1 associated protein 1.

genetic distinctions between the high- and low-risk groups, we conducted comparative analyses which identified four genes exhibiting significant differential mutation frequencies, including the previously highlighted pair (Figure 7B). Among these, BAP1 emerged as the most consequential gene, consistent with its well-established role in UVM pathogenesis. Reduced expression or functional loss of BAP1 has been implicated in enhancing the metastatic capacity of UVM cells[27]. Additionally, other genes such as *SF3B1*, *EIF1AX*[28], and *GNAQ/GNA11*[29] have garnered considerable attention for their critical involvement in melanoma metastasis, supported by extensive prior studies. The mutations affecting these four genes are therefore likely contributors to the progression and aggressiveness of UVM.

To gain finer resolution of mutation landscapes, we mapped mutation sites within key genes, highlighting affected functional domains. We also analyzed patterns of co-occurrence and mutual exclusivity among the top 20 frequently

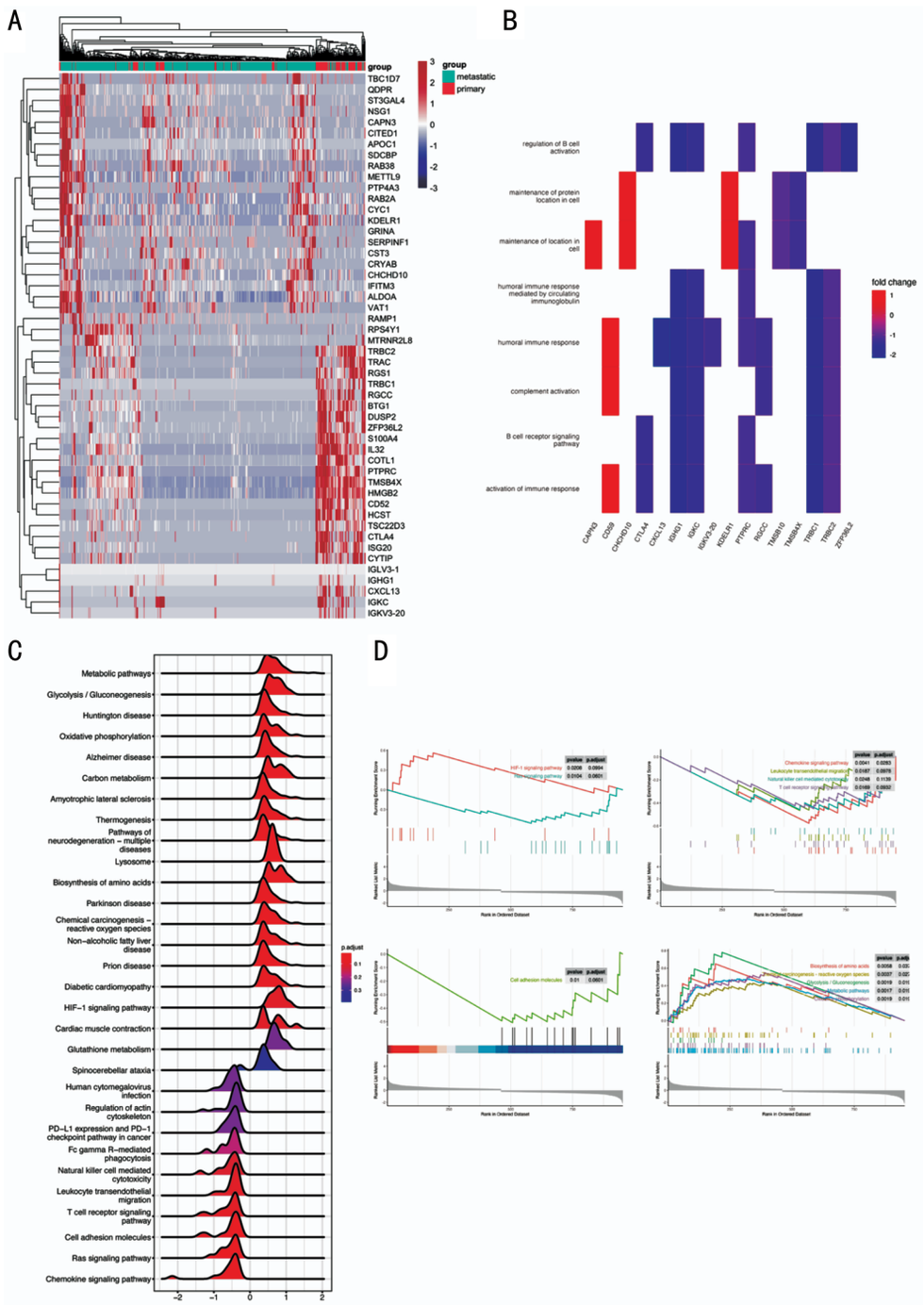

Figure 6 Analysis of the cell cluster identified by the key genes A: Heatmap illustrating the top 25 upregulated and downregulated DEGs between primary and metastatic tumor cells within the Tumor cells-2 cluster. B: GO enrichment analysis of these DEGs, visualized using the enrichplot package in R. C: KEGG pathway analysis conducted *via* the clusterProfiler R package to explore biological processes associated with the DEGs. D: GSEA identified four functional modules significantly enriched in metastatic UVM cells, encompassing cell migration, immune regulation, metabolic pathways, and chemical carcinogenesis (P<0.05). DEGs: Differentially expressed genes; GO: Gene Ontology; KEGG: Kyoto Encyclopedia of Genes and Genomes; GSEA: Gene Set Enrichment Analysis; UVM: Uveal melanoma.

mutated genes across risk groups, visualized through color-coded matrices, where green indicates co-occurrence and brown denotes mutual exclusivity (Figure 7C). Notably, *GNAQ* and *GNA11* displayed a strong mutual exclusivity pattern, corroborating earlier reports. These findings collectively offer valuable insights into the molecular underpinnings of UVM. Moreover, the CNV profiles were extensively characterized (Figure 7D). Positive G-scores signified regions of chromosomal amplification, whereas negative scores indicated deletions, with the magnitude of scores reflecting the significance of these alterations[30]. Aggregated CNV data encompassing genes from our signature set and differentially mutated candidates were also assessed across samples (Figure 7E). Interestingly, genes in the high-risk cohort showed

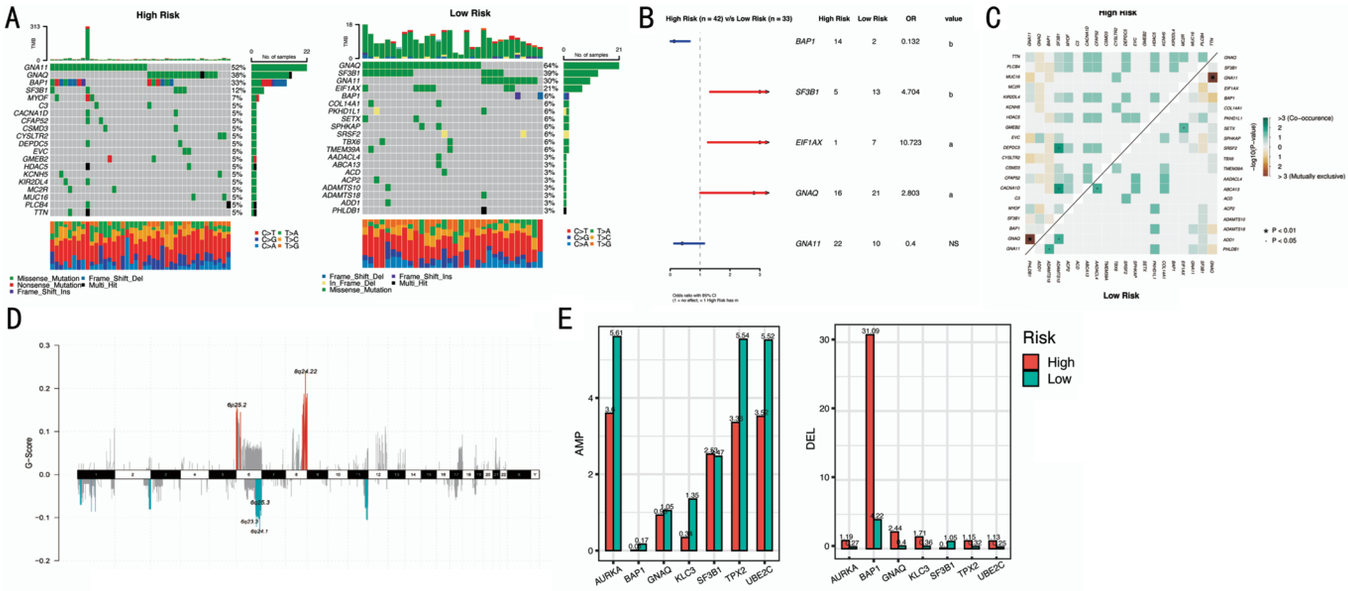

Figure 7 Genetic alterations of the different risk groups divided by gene signature A: Waterfall plots displaying the mutation landscapes of the high- (left) and low-risk (right) groups. B: Forest plot showing the significantly different mutated genes between risk groups. Statistical significance is denoted as ns (not significant), [a]*P*<0.05, [b]*P*<0.01. C: The coincident and exclusive associations across the top mutated genes in high- and low-risk groups. D: The distribution of CNV features about gene amplification and deletion across all chromosomes. Positive G-Score represented amplification while negative represented deletion. E: The sum of amplification and deletion results of gene signature and significantly different mutation genes. CNV: Copy number variation; UVM: Uveal melanoma; G-Score: Score representing amplification (positive) or deletion (negative).

reduced amplification levels compared to those in the low-risk group, while deletions were more pronounced in the high-risk patients. This inverse relationship suggests that gene deletions may contribute to increased metastatic risk in UVM, whereas amplifications could have a protective effect. Furthermore, significant differences in CNV deletions were observed for several key genes, including BAP1, GNAQ, AURKA, TPX2, and UBE2C between the two risk categories.

DISCUSSION

UVM exhibits aggressive behavior, often accompanied by occult micro-metastases that remain undetected at initial diagnosis[31-32]. While therapeutic options have limited efficacy in advanced metastatic UVM, early clinical interventions in non-metastatic or low-risk cases have demonstrated improved patient outcomes[33]. Consequently, distinguishing metastatic potential is of high clinical relevance. Previous studies have delineated gene expression profiles stratifying UVM into class 1 (low-risk) and class 2 (high-risk) tumors[34]. Leveraging bulk RNA-sequencing data, our study focused on elucidating critical molecular regulators linked to patient prognosis and TME immune infiltration. Integration of PPI networks with TCGA-UVM expression and clinical data enabled identification of a seven-gene signature significantly associated with metastatic risk and survival. Notably, differences in immune cell infiltration mirrored genetic disparities between high- and low-risk tumors, highlighting the interplay between genomic alterations and TME characteristics.

UVM tissues comprise both tumor cells and heterogeneous immune populations, with composition varying across tumor types. Disruption of immune surveillance can contribute to UVM metastasis. Using the ssGSEA package and ESTIMATE algorithm, we quantified immune cell infiltration and calculated matrix and immune scores to characterize the TME. Our analyses revealed that immune and stromal activities were reduced in high-risk UVM tumors, highlighting potential biomarkers and therapeutic targets, and providing insights into the limited efficacy of current immunotherapies. Notably, single molecules may induce immune tolerance by remodeling the TME to facilitate immune evasion[35]. The mechanisms by which multiple key molecules orchestrate immune cell infiltration in UVM remain incompletely understood. Integrative analyses of these molecules illuminate the complex regulation of antitumor immune responses and may guide the development of immunotherapies targeting TME heterogeneity[36]. Our results further indicate that tumor genomic alterations influence immune infiltration patterns: compared with class 1 tumors, immune cell abundance in class 2 tumors was partially reduced. Moreover, expression levels of the identified key molecules significantly correlated with immune cell infiltration, consistent with survival analyses, supporting their potential role in modulating the TME.

Employing LASSO Cox regression, we crafted a risk score

using seven key molecules. This score effectively differentiated high and low-risk groups in UVM patients, establishing itself as an independent prognostic factor, confirmed by multivariate Cox regression analysis. It is noteworthy that these core genes have yet to be reported in direct association with UVM; nevertheless, they have been extensively scrutinized in the context of other malignancies. For instance, the *AURKA* gene's activation is indispensable for orchestrating cell division processes through mitotic regulation, implying its potential as a target for cancer therapeutics. In fact, certain small molecules aimed at inhibiting AURKA have already been unearthed[37]. Additionally, DLGAP5, a microtubule-associated protein, exhibits the capacity to silence the Wnt/β-catenin signaling pathway in endometrial cancer cells when knocked down[38]. While these genes hold promise as potential indicators of clinical prognosis in UVM, it is essential to emphasize the need for further in-depth research to unveil their precise roles within the context of ocular cancer.

Then, we explored the expression patterns of these genes on the single-cell-level gene sequencing dataset and were surprised to find that these gens were concentrated in the same cluster. And this cluster is one tumor cell population of UVM with loss of BAP1 expression, which means that there is a premature termination of the BAP1 protein (p.Q322fsX100) in UVM with high metastasis risk class 2[36]. Subsequent differential gene annotation also unveils intriguing pathway features implicated in this highly metastatic signature of tumor cells. These pathways encompass alterations in metabolism, immune response, and cell adhesion. Notably, the loss of BAP1 in samples from UVM patients correlates with the upregulation of gene expression related to several cell adhesion molecules, including E-cadherin (CDH1), cell adhesion molecule 1 (CADM1), and syndecan-2 (SDC2)[39]. Similarly, UBE2C demonstrates a positive association with the adhesion molecule N-cadherin, matrix metalloproteinases, and cyclin-related genes, indicating its close connection to cell adhesion processes[40]. Consequently, the heightened metastatic potential of UVM appears to be the result of a complex interplay among multiple genes and integrated pathways.

To elucidate the molecular underpinnings of the seven-gene signature, we conducted comprehensive analyses of somatic mutations and copy number variations across distinct UVM risk cohorts, assessing their impact on tumor pathogenesis and progression. *BAP1* mutation exhibited pronounced divergence, reaffirming its critical role in UVM development[41], while *GNAQ* and *GNA11*, encoding G protein subunits, were also prominently implicated, with functional relevance supported by GeneCards, highlighting the contribution of G-protein signaling dysregulation to UVM susceptibility and metastasis. Mechanistically, the signature was preferentially enriched in BAP1-deficient tumor clusters, consistent with BAP1's role in chromatin remodeling and transcriptional regulation[42-43]. Key genes within the panel, including *UBE2C* and *AURKA*, are linked to cell cycle control and chromosomal instability, suggesting they act as downstream effectors of BAP1 loss. Concurrently, *GNAQ* and *GNA11* mutations, which activate MAPK and YAP signaling[44-45], converge on transcriptional programs overlapping with components of the seven-gene signature, whereas the signature's presence in tumors lacking *SF3B1* or *EIF1AX* mutations indicates partial independence from these canonical drivers, reflecting broader oncogenic and microenvironmental dysregulation. Collectively, these findings indicate that the seven-gene signature integrates downstream effects of canonical UVM drivers with parallel regulatory pathways, forming a convergent molecular phenotype shaped by BAP1-mediated transcriptional alterations, GNAQ/GNA11-driven proliferative signaling, and additional independent mechanisms, thereby reinforcing its prognostic value and providing mechanistic insights into tumor progression and immune microenvironment modulation, as illustrated in.

This study has several limitations. First, although preliminary *in vitro* validation of the seven key genes was performed using UVM cell lines, *in vivo* experiments and comprehensive functional assays are required to fully elucidate their mechanistic roles. Second, the limited clinical annotations in publicly available datasets constrained the analysis of clinicopathological variables, which may impact the predictive performance of the riskscore model. Validation in larger and more extensively annotated patient cohorts would further substantiate the prognostic utility of this seven-gene signature. Notably, our findings emphasize the novelty of the signature by integrating prognostic significance with immune microenvironment characteristics, revealing robust associations between the seven-gene panel and immune cell infiltration patterns. By combining systematic bioinformatics analyses with experimental validation, this study establishes the seven-gene riskscore as a robust and independent prognostic biomarker in UVM. Beyond its prognostic value, the signature provides mechanistic insights into tumor progression and immune modulation, offering a rational framework to guide the development of targeted immunotherapeutic strategies, including precision combination regimens and personalized interventions, thereby advancing the implementation of precision medicine in UVM management.

ACKNOWLEDGEMENTS

Authors' Contributions: Guo YM conceived and designed the study, performed data analysis, conducted cell experiments, and drafted the manuscript. Bai ZP contributed to data collection, investigation, and visualization. Wang JQ conducted formal data analysis and participated in manuscript

revision. Huang J assisted in cell culture and experimental implementation. Wei JH was involved in data curation and manuscript editing. Han YJ contributed to data analysis, figure preparation, and critical revision of the manuscript. Liu Y contributed to study design, supervised data analysis, and coordinated the research process. Ye L provided overall supervision, acquired funding, and approved the final version of the manuscript.

Data Availability Statement: Generated Statement: Publicly available datasets were analyzed in this study. This data can be found here: The Cancer Genome Atlas will be available from https://portal.gdc.cancer.gov/. The names of the repository/repositories and accession number(s) can be found below: https://www.ncbi.nlm.nih.gov/geo/query/acc.cgi?acc=GSE13982; https://www.ncbi.nlm.nih.gov/geo/query/acc.cgi acc=GSE73652.

Foundations: Supported by the National Natural Science Foundation of China (No.82460215); National Natural Science Foundation of China Pre-experimental Project (No.2025GZRYSY006); 2025 Youth Training Project of the Xi'an Municipal Health Commission (No.2025qn05); Xi'an Medical Research-Discipline Capacity Building Project (No.23YXYJ0002); Key R&D Plan of Shaanxi Province: Key Industrial Innovation Chain (Cluster)-Social Development Field (No.2022ZDLSF03-10); Research Incubation Fund of Xi'an People's Hospital (Xi'an Fourth Hospital; No.LH-13).

Conflicts of Interest: Guo YM, None; **Bai ZP,** None; **Wang JQ,** None; **Huang J,** None; **Wei JH,** None; **Han YJ,** None; **Liu Y,** None; **Ye L,** None.

REFERENCES

1 Jager MJ, Shields CL, Cebulla CM, *et al*. Uveal melanoma. *Nat Rev Dis Primers* 2020;6:24.

2 Chattopadhyay C, Kim DW, Gombos DS, *et al*. Uveal melanoma: From diagnosis to treatment and the science in between. *Cancer* 2016;122(15):2299-2312.

3 Wang H, Luo JT, Tao YX, *et al*. A 10-year fight for vision in a patient with recurrent uveal melanoma: a case report. *Int J Ophthalmol* 2023;16(10):1718-1720.

4 Yang J, Manson DK, Marr BP, *et al*. Treatment of uveal melanoma: where are we now? *Ther Adv Med Oncol* 2018;10:1758834018757175.

5 Tao YX, Li HW, Luo JT, *et al*. Regional chemotherapy for uveal melanoma liver metastases. *Int J Ophthalmol* 2023;16(2):293-300.

6 Karlsson JW, Sah VR, Olofsson Bagge R, *et al*. Patient-derived xenografts and single-cell sequencing identifies three subtypes of tumor-reactive lymphocytes in uveal melanoma metastases. *Elife* 2024;12:RP91705.

7 Arturi FJ, Arons D, Murphy NJ, *et al*. The effects of radiation therapy on the ocular apparatus: implications for management. *Cancers* (*Basel*) 2025;17(16):2605.

8 Reiter S, Schroeder C, Broche J, *et al*. Successful treatment of metastatic uveal melanoma with ipilimumab and nivolumab after severe progression under tebentafusp: a case report. *Front Oncol* 2023;13:1167791.

9 Chen YN, Xiu JY, Zhao HQ, *et al*. Prognostic prediction model for Chinese uveal melanoma patients based on matrix metalloproteinase-2 and-28 expression levels in the tumor. *Int J Ophthalmol* 2025;18(5):765-778.

10 Yang S, Liu T, Nan HM, *et al*. Comprehensive analysis of prognostic immune-related genes in the tumor microenvironment of cutaneous melanoma. *J Cell Physiol* 2020;235(2):1025-1035.

11 Pan Y, Yu Y, Wang X, Zhang T. Tumor-associated macrophages in tumor immunity. *Front Immunol* 2020;11:583084.

12 Alonso-Agudo T, Johansson J, Ståhlberg A, *et al*. Cellular and molecular characterization of γδ T cells in peripheral blood from patients with metastases from cutaneous and uveal melanoma. *Front Immunol* 2025;16:1564333.

13 Menéndez V, Solórzano JL, García-Cosío M, *et al*. Immune and stromal transcriptional patterns that influence the outcome of classic Hodgkin lymphoma. *Sci Rep* 2024;14(1):710.

14 Grigoruta M, Kong XH, Qin Y. Advances and challenges in immunotherapy for metastatic uveal melanoma: clinical strategies and emerging targets. *J Clin Med* 2025;14(14):5137.

15 Gelmi MC, Gezgin G, Kapiteijn E, *et al*. Tumour progression shows decrease in PD-L1 expression in matched metastases/primary uveal melanomas. *Acta Ophthalmol* 2025. Author Correction: Immune and stromal transcriptional patterns that influence the outcome of classic Hodgkin lymphoma. *Sci Rep* 2024;14(1):27537.

16 Luo H, Ma C. Identification of prognostic genes in uveal melanoma microenvironment. *PLoS One* 2020;15(11):e0242263.

17 Li K, Sun LF, Wang YN, *et al*. Single-cell characterization of macrophages in uveal melanoma uncovers transcriptionally heterogeneous subsets conferring poor prognosis and aggressive behavior. *Exp Mol Med* 2023;55(11):2433-2444.

18 Ritchie ME, Phipson B, Wu D, *et al*. Limma powers differential expression analyses for RNA-sequencing and microarray studies. *Nucleic Acids Res* 2015;43(7):e47.

19 Szklarczyk D, Franceschini A, Wyder S, *et al*. STRING v10: protein-protein interaction networks, integrated over the tree of life. *Nucleic Acids Res* 2015;43(Database issue):D447-D452.

20 Barbie DA, Tamayo P, Boehm JS, *et al*. Systematic RNA interference reveals that oncogenic KRAS-driven cancers require TBK1. *Nature* 2009;462(7269):108-112.

21 Yoshihara K, Shahmoradgoli M, Martínez E, *et al*. Inferring tumour purity and stromal and immune cell admixture from expression data. *Nat Commun* 2013;4:2612.

22 Shang FJ, Wang YF, Shi ZX, *et al*. Development of a signature based on eight metastatic-related genes for prognosis of GC patients. *Mol Biotechnol* 2023;65(11):1796-1808.

23 Jiang GQ, Zhao YP, Zhang YH, *et al*. Unraveling the prognostic significance and molecular mechanisms of HKDC1 in cancer *via*

integrated multi-omics and experimental validation. *Pathol Res Pract* 2025;272:156101.

24 Mayakonda A, Lin DC, Assenov Y, *et al*. Maftools: efficient and comprehensive analysis of somatic variants in cancer. *Genome Res* 2018;28(11):1747-1756.

25 Mermel CH, Schumacher SE, Hill B, *et al*. GISTIC2.0 facilitates sensitive and confident localization of the targets of focal somatic copy-number alteration in human cancers. *Genome Biol* 2011;12(4):R41.

26 Ye Z, Yuan J, Yi Q, *et al*. SNP rs615552 and lncRNA CDKN2B-AS1 influence brain cancer pathogenesis through multi-omic mechanisms. *Sci Rep* 2025;15(1):27490.

27 Li W, Nie AQ, Li Q, *et al*. Bioinformatic analysis of differentially expressed genes and screening of hub genes in uveal melanoma cells with BRCA1-associated protein 1 related protein 1 depletion. *J Biomed Nanotechnol* 2020;16(8):1205-1218.

28 Londin E, Magee R, Shields CL, *et al*. IsomiRs and tRNA-derived fragments are associated with metastasis and patient survival in uveal melanoma. *Pigment Cell Melanoma Res* 2020;33(1):52-62.

29 Banimohammad M, Khalafi P, Gholamin D, *et al*. Exploring recent advances in signaling pathways and hallmarks of uveal melanoma: a comprehensive review. *Explor Target Anti Tumor Ther* 2025:1002306.

30 Shoshani O, Brunner SF, Yaeger R, *et al*. Chromothripsis drives the evolution of gene amplification in cancer. *Nature* 2021;591(7848): 137-141.

31 Hagström A, Kal Omar R, Williams PA, *et al*. The rationale for treating uveal melanoma with adjuvant melatonin: a review of the literature. *BMC Cancer* 2022;22(1):398.

32 Rantala ES, Hernberg MM, Piperno-Neumann S, *et al*. Metastatic uveal melanoma: The final frontier. *Prog Retin Eye Res* 2022;90:101041.

33 Krohn J, Vinnem LIH, Jansson RW, *et al*. Fundus hypopigmentation and choroidal thinning associated with tebentafusp therapy: report of a case and literature review. *BMC Ophthalmol* 2025;25(1):464.

34 Fuentes-Rodriguez A, Mitchell A, Guérin SL, *et al*. Recent advances in molecular and genetic research on uveal melanoma. *Cells* 2024;13(12):1023.

35 Shi XY, Xia SL, Chu YM, *et al*. CARD11 is a prognostic biomarker and correlated with immune infiltrates in uveal melanoma. *PLoS One* 2021;16(8):e0255293.

36 Wu Q, Wang L, Wei HG, *et al*. Integration of multiple key molecules in lung adenocarcinoma identifies prognostic and immunotherapeutic relevant gene signatures. *Int Immunopharmacol* 2020;83:106477.

37 Du RJ, Huang CT, Liu KD, *et al*. Targeting AURKA in Cancer: molecular mechanisms and opportunities for Cancer therapy. *Mol Cancer* 2021;20(1):15.

38 Chen RP, Liu J, Hu J, *et al*. DLGAP5 knockdown inactivates the Wnt/β-catenin signal to repress endometrial cancer cell malignant activities. *Environ Toxicol* 2023;38(3):685-693.

39 Baqai U, Purwin TJ, Bechtel N, *et al*. Multi-omics profiling shows BAP1 loss is associated with upregulated cell adhesion molecules in uveal melanoma. *Mol Cancer Res* 2022;20(8):1260-1271.

40 Kariri Y, Toss MS, Alsaleem M, *et al*. Ubiquitin-conjugating enzyme 2C (UBE2C) is a poor prognostic biomarker in invasive breast cancer. *Breast Cancer Res Treat* 2022;192(3):529-539.

41 Zheng GP, Shi JH, Li Q, *et al*. BAP1 inactivation promotes lactate production by leveraging the subcellular localization of LDHA in melanoma. *Cell Death Discov* 2024;10:483.

42 Xia YK, Zeng YR, Zhang ML, *et al*. Tumor-derived neomorphic mutations in ASXL1 impairs the BAP1-ASXL1-FOXK1/K2 transcription network. *Protein Cell* 2021;12(7):557-577.

43 Ouyang SM, Shi S, Ding W, *et al*. Neuropeptide precursor VGF promotes liver metastatic colonization of Gαq mutant uveal melanoma by facilitating tumor microenvironment *via* paracrine loops. *Adv Sci* 2024;11(46):2407967.

44 Li S, Liu Y, Wu X, *et al*. UBE2C: a potential therapeutic target and prognostic biomarker for prostate cancer patients. *Funct Integr Genom* 2025;25(1):159.

45 Alqussair F, Elshal M, Makled MN, *et al*. The AURKA-selective inhibitor alisertib attenuates doxorubicin-induced hepatotoxicity in mice *via* modulation of IL-17A/NF-κB and STAT3 signaling pathways. *Pharmaceuticals* (*Basel*) 2025;18(8):1201.